CHEMISTRY OF MATERIALS

Article

pubs.acs.org/cm

Bioresponsive Controlled Drug Release Based on Mesoporous Silica Nanoparticles Coated with Reductively Sheddable Polymer Shell

Baisong Chang,[†] Dan Chen,[†] Yang Wang,[†] Yanzuo Chen,[‡] Yunfeng Jiao,[†] Xianyi Sha,[‡] and Wuli Yang*,[†]

[†]State Key Laboratory of Molecular Engineering of Polymers, Department of Macromolecular Science, Fudan University, No. 220 Handan Road, Shanghai 200433, China

[‡]Key Laboratory of Smart Drug Delivery (Fudan University), Ministry of Education & PLA, Department of Pharmaceutics, School of Pharmacy, Fudan University, No. 826 Zhangheng Road, Shanghai 201203, China

ABSTRACT: The design of bioresponsive controlled drug delivery systems is a promising approach in cancer therapy, but it still is a major challenge capable of optimum therapeutic efficacy, i.e. no premature drug leakage in blood circulation while having a rapid and complete release in tumor tissues. In this work, a kind of PEGylated core/shell structured composite nanoparticle was developed via precipitation polymerization, where a disulfide-cross-linked poly(*N*-vinylcaprolactam-*co*-methacrylic acid) (P(VCL-*s*-*s*-MAA)) polymer shell was created to act as sheddable thermo/pH-sensitive gatekeepers, and a carboxylic acid modified mesoporous silica nanoparticles (MSN-COOH) core was applicable as an accessible reservoir to encapsulate high drug doses. At physiological conditions, the P(VCL-*s*-*s*-MAA)-PEG shell underwent a distinct transition from a swollen state in pH 7.4 to a collapsed state in pH 5.0. Though sufficiently stable in water, composite nanoparticles were prone to fast dissociation and rupture when subjecting to 10 mM glutathione (GSH), due to the shedding of polymer walls through reductive cleavage of intermediate disulfide bonds, so that the polymer shell was active in moderating the diffusion of embedded drugs in-and-out of MSN channels. The cumulative *in vitro* release of DOX-loaded composite nanoparticles allowed a low trace of DOX diffusion below volume phase transition temperature (VPTT) and a significant release rate above its VPTT, while the most rapid and perfect release was achieved under a reductive environment (pH 6.5 and 10 mM GSH), mimicking that of intracellular cytosol compartments. The *in vitro* cell assay of blank carriers to normal cells indicated that the composite nanoparticles were suitable as drug carriers, but DOX-loaded carriers had a similar intensive toxicity to cancer cells compared with free DOX. Therefore, these stimuli-responsive composite nanoparticles with a reductively sheddable and thermo/pH-responsive polymer shell gate could, in principle, be applied for *in vivo* cancer therapy, and synergistic drug delivery can be accomplished "just in time" in a precise event over the location.

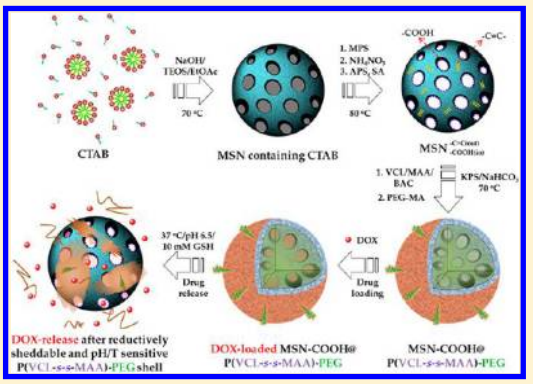

KEYWORDS: *thermo/pH-responsive, shell-sheddable, core/shell, MSN, controlled drug release*

1. INTRODUCTION

The development of stimuli-responsive nanomaterials for cancer treatment has been receiving extensive attention in recent years and now has become a principal field in medical research.[1−4] Among various dedicated materials for drug delivery applications, the burgeoning interest in mesoporous silica nanoparticles (MSN) has been greatly spurred since they exhibit more flexible and robust properties, including excellent chemical stability, easily modification, and prominent biocompatibility.[5−7] Moreover the large surface area and pore volume for MSN ensure facile transporting as well as high loading of various guest molecules.[8−10] Although the utilization of MSN has validated great potential in delivering drugs, this technique is facing tremendous challenges. In particular, conventional pure MSN materials are unintelligent carriers and usually bestow a drug-release profile that is not in favor of achieving optimal drug availability inside cancer cells.[11] That is a premature and burst release for the loaded drugs within several hours after intravenous administration, followed by a slow diffusional and incomplete drug release providing an unsatisfied local therapeutic efficacy.

To date, rapid advances in the elaborate synthesis of bioresponsive MSN drug delivery systems are particularly appealing for opening or closing of the mesoporous entrance by surface modification or decoration.[12−14] The conceptual "on-demand" controlled delivery of encased cargos can be actuated upon exposure to internal or external stimulants. Lin et al. used CdS or Fe_3O_4 as a gate to demonstrate the chemical reduction activated release from MSN in the aqueous environments.[15,16] The potential utility of these modified MSN was still limited because of the unwanted possible cytotoxicity of unlinked inorganic nanoparticles gates. To tackle this issue, one reliability strategy is to fabricate environment responsive polymer-coated MSN systems.[17] Typical biological intervention

Received: November 17, 2012
Revised: January 24, 2013
Published: January 30, 2013

exploited for the favored drug release includes pH and temperature. For example, most of the cancer tissues have lower extracellular pH values (6.0−7.0) than normal tissues and the bloodstream (pH 7.4) but still drop inside cells especially in endosome (pH 4.5−5.5).[1] The local character for certain malignancies also shows a distinct hyperthermia.[18] Additionally, it is generally accepted that cytosol always contain 2 to 3 orders higher level of glutathione tripeptide (approximate 0.5−10 mM) than extracellular fluids (2−20 μM).[19] Consequently, these features could be applied for feasibly creating multisensitive MSN-based carriers that intelligently distinguish microenvironment difference between normal and tumor tissues, achieving a better targeting and treatment efficacy. Indeed, by utilizing variations in pH or temperature, efforts for the development of responsive drug carriers have recently been made.[20−23] However, most of these were limited to monostimulus and failed to meet "zero premature release" in the bloodstream. In a previous work, we had reported that a combination of thermo/pH-sensitive poly(*N*-isopropylacrylamide-*co*-methacrylic acid) coated magnetic MSN composite nanoparticles could be used in drug delivery with a tailored release manner: a low level of drug leakage below volume phase transition temperature (VPTT) and a high release above VPTT.[24] In the optimistic view, it can precisely match the actual physiological needs at the proper time and site. Owing to the cross-linked polymer shell partially blocking the entrance toward mesopores, this type of drug carrier with a chemical stable polymer shell cannot realize a complete drug release once reaching a designated target, which leads to the insufficient intracellular drug availability for killing cancer cells. Therefore, the design of a delivery system with better release properties is still of paramount importance.

One of the most promising strategies is to decompose the polymer shell that responds to the drug release process. Herein, we described the preparation of a core/shell structured multisensitive composite nanoparticle, which comprised PEG corona to depress nonspecific binding, thermo/pH-coupling responsive poly(*N*-vinylcaprolactam-*s*-*s*-methacrylic acid) (P(VCL-*s*-*s*-MAA)) shell with a disulfide-cross-linked network to work as gatekeeper, and MSN core to payload anticancer drugs. Our assessments indicated that volume phase transition of MSN-COOH@P(VCL-*s*-*s*-MAA)-PEG could be precisely tuned by the mass ratio of VCL to MAA. The effective shedding and rupture of P(VCL-*s*-*s*-MAA)-PEG integrity through reductive damage were also documented. Such well-fabricated drug carriers had been engineered to respond to slight variations in the simulated physiological environments. The multisensitive composite nanoparticles were applicable to load high DOX content and exhibited an elegant release fashion: extremely low premature release at pH 7.4, a rapid release upon reaching the reduced pH 6.5 and 5.0 but the most rapid and complete drug release when pH 6.5 and 10 mM GSH were both applied simultaneously. Subsequently, cytotoxicity of blank composite nanoparticles to normal cells and DOX-loaded carriers to cancer cells were also evaluated.

2. EXPERIMENTAL SECTION

2.1. Materials. *N*-Vinylcaprolactam (VCL, 99%) and poly(ethylene glycol) methyl ether methacrylate solution (PEG-MA, Mn 2000, 50 wt % in H_2O) were obtained from Sigma-Aldrich. 3-(Trimethoxylsilyl) propyl methacrylate (MPS, 99%), *N*,*N*′-bis(acryloyl)cystamine (BAC, 98%), and glutathione (GSH, 98%) were purchased from Fluka and used as received. Methacrylic acid (MAA), tetraethyl orthosilicate (TEOS), cetyltrimethylammonium bromide (CTAB), ethyl acetate (EtOAc), ammonium nitrate (NH_4NO_3), succine anhydride (SA), 3-aminopropyltriethoxysilane (APS), potassium persulfate (KPS), and sodium dodecyl sulfate (SDS) were analytical grade and commercially available products. All the chemicals were used without any additional purification. Doxorubicin in the form of hydrochloride salt (DOX) was obtained from Beijing Huafeng United Technology Company. VCL was recrystallized three times from its melt at room temperature, and the resultant crystal was washed with cold methanol and dried under vacuum. MAA was distilled under reduced pressure prior to use, and KPS was recrystallized twice from water.

2.2. Preparation of MSN-COOH@P(VCL-*s*-*s*-MAA)-PEG Composite Nanoparticles. The experimental procedure was a slight modification of a method reported previously.[25] The details were described as follows. Initially 1 g of CTAB was weighed and dissolved in 500 mL of deionized water in a 1 L flask. Then, 3 mL of 2 M NaOH (aq) as the base catalyzer of the sol−gel reaction was added. The above mixture was heated continuously to 70 °C under a vigorous mechanical stirring, followed by the addition of TEOS (5 mL). After 1 min, 5 mL of EtOAc was successively added, and the resulting mixture was rapidly stirred for another 30 s. In the next step, the stirring was stopped quickly, and the reaction was allowed to age for an additional 2 h. The acquired white precipitate was isolated by centrifugation and repeatedly washed with ethanol. Finally, the above CTAB-containing product was dispersed directly into 200 mL of ethanol solution with 0.5 mL of MPS. After having been stirred at 25 °C for 12 h, the structure-templating CTAB surfactants were removed from mesopores via ion exchange.[26] A suspension of the as-synthesized product was stirred for 30 min at 60 °C in 300 mL of ethanol containing 4 g of NH_4NO_3. The template-removed solid was collected and washed by centrifugation. The obtained MPS-modified MSN (denoted as $MSN^{-C=C-(out)}$) was then dispersed again in ethanol and diluted to 1 wt % for subsequent use.

To adjust DOX-surface interaction, mesoporous channels were functionalized with organic silanes containing an amino group ($-NH_2$) through a postgrafting method.[27] Typically, 1 g of $MSN^{-C=C-(out)}$ was dispersed in 250 mL of ethanol. After the addition of APS (6 mmol), the mixture was stirred moderately at 80 °C for 6 h. The precipitate was collected by centrifugation and then added directly in the DMF solution of SA (250 mL, 2 wt %). The mixture was stirred for 24 h at room temperature. After that, the obtained sample was centrifuged, washed with ethanol, and dried under vacuum. The name of the synthetic specimen was designated as $MSN^{-C=C-(out)}_{-COOH(in)}$.

Core/shell polymer coated MSN composite nanoparticles were synthesized by precipitation polymerization in the presence of $MSN^{-C=C-(out)}_{-COOH(in)}$ as seeds. In a typical route, a solution of 180 mg of VCL, 20 mg of MAA, 10 mg of BAC, 5 mg of $NaHCO_3$ and 3 mg of SDS dissolved in 45 mL of deionized water was prepared in a three-neck flask equipped with a reflux condenser. Five g of 1 wt % $MSN^{-C=C-(out)}_{-COOH(in)}$ dispersion was then added. The mixture was heated up to 70 °C and bubbled with N_2 to exclude O_2. After mechanical stirring at 200 rpm for more than 0.5 h, 1 mL of KPS solution (5 mg/mL) was rapidly added to initiate the polymerization. The reaction was continued for 0.5 h with continuous stirring. Afterward, a shot of PEG-MA solution (0.3 mL) was added into the reaction mixture, and the mixture was polymerized for another 6 h. The latex was cooled down to 25 °C. Upon isolation at 12000 rpm for 5 min, the precipitate was dispersed in deionized water, and the resulted emulsion was dialyzed (molecular weight cut off = 14000) against water for 5 days to eliminate any unreacted monomers. The different feed mass ratios of VCL/MAA = (100-X)/X (X increased from 0 to 20) were prepared by the same procedure, and composite nanoparticles were named as MSN-COOH@P(VCL-*s*-*s*-MAA)-PEG/X correspondingly.

2.3. Reduction-Triggered Shedding of MSN-COOH@ P(VCL-*s*-*s*-MAA)-PEG Composite Nanoparticles. Under a N_2 flow, a predetermined amount of GSH was introduced to a cuvette with 1.5 mL of MSN-COOH@ P(VCL-*s*-*s*-MAA)-PEG composite nanoparticles (0.15 M, pH 6.5), which leads to a final GSH concentration of 10 mM. The cuvette was then sealed and placed at 37 °C with a

dx.doi.org/10.1021/cm3037197 | *Chem. Mater.* 2013, 25, 574−585

Scheme 1. Illustration of the Synthetic Process for Core/Shell Hybrid Mesoporous Silica Nanoparticles (MSN) Coated with Reductively Sheddable and Thermo/pH-Sensitive P(VCL-*s*-*s*-MAA)-PEG Shell by Precipitation Polymerization

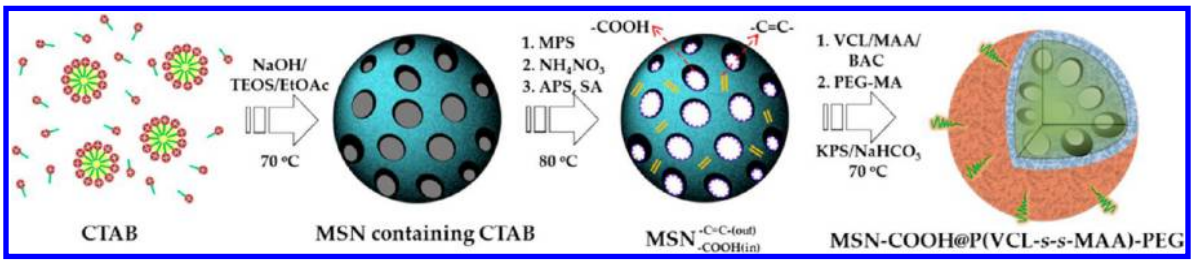

rotation of 200 rpm. At alternate intervals, the hydrodynamic diameter was tested by DLS in time. For TEM measurement, the mixture was isolated to collect the solid samples and then resuspended again with water in a diluted concentration. Meanwhile, the supernatant was used to test the molecular weight of the reductively sheddable polymer chains using a matrix-assisted laser desorption/ionization time-of-flight (MALDI-TOF) instrument.

2.4. DOX Loading and Release. 0.1 M NaOH (aq) was added in DOX solution (1 mg/mL) reaching the desired pH of ~8.5. Five mg of MSN-COOH@ P(VCL-*s*-*s*-MAA)-PEG was ultrasonically dispersed in 1.5 mL of DOX solution and stirred at 25 °C lasting 12 h. Then it was centrifuged to bring DOX-loaded carriers together and gently washed with deionized water twice to remove the surface adsorption of DOX. The amount of DOX in the MSN-COOH@P(VCL-*s*-*s*-MAA)-PEG carrier was calculated by subtracting the mass of DOX in the supernatant from the total mass of drug initial solution by UV−vis at 480 nm using a pre-established calibration curve.

For the thermo/pH-dependent guest DOX release studies, various buffer solutions with the same NaCl concentration of 0.15 M were chosen: sodium acetate buffer for pH 5.0, phosphate buffer for pH 6.5 and 7.4. For a direct quantitative measurement of releasing efficiency in the presence of reductive agents, the release profile was performed in a pH 6.5, 0.15 M NaCl, and 10 mM GSH media. DOX-loaded MSN-COOH@P(VCL-*s*-*s*-MAA)-PEG nanoparticles were dispersed in 2 mL of buffer and transferred into a dialysis bag. Then it was kept in 200 mL of buffer and gently shaken at 37 °C. At selected timed intervals, 1 mL of solution was withdrawn and analyzed by UV−vis. To retain a constant volume, 1 mL of fresh buffer was added after each sampling. All the drug release results were averaged with three measurements.

2.5. *In Vitro* Cell Assay. The cytotoxicity assay of DOX-loaded MSN-COOH@ P(VCL-*s*-*s*-MAA)-PEG against MCF-7 (human breast adenocarcinoma, cancer cells) and MSN-COOH@P(VCL-*s*-*s*-MAA)-PEG against HEK 293 (human embryonic kidney, normal cells) were assessed by the standard MTT assay. MCF-7 cells and 293 cells were cultured in a DMEM medium supplemented with 10% (v/v) fetal bovine serum, 2 mM L-glutamine, 100 U/mL of penicillin, and 100 mg/mL of streptomycin at 37 °C and 5% CO_2.

For the MTT assay, MCF-7 cells were seeded in 96-well plates at a density of 5000 viable cells per well and incubated for 24 h to allow cell attachment. Then the cells were incubated with free DOX, DOX-loaded MSN-COOH @P(VCL-*s*-*s*-MAA)-PEG, and blank MSN-COOH@P(VCL-*s*-*s*-MAA)-PEG at indicated concentrations, respectively. After 48 h, the medium were replaced with fresh DMEM containing MTT (5 mg/mL), and the cells were incubated for an additional 4 h. Upon the removal of MTT solution, the purple formazan crystals generated by live cells were dissolved with DMSO. The relative cell viability was determined by comparing the absorbance at 570 nm with control wells containing only cell culture medium. The results were expressed as mean values of three measurements. The same process of cytotoxicity to MSN-COOH @P(VCL-*s*-*s*-MAA)-PEG against 293 cells was implemented as mentioned above.

The cellular uptake and intracellular release behaviors of DOX-loaded composite nanoparticles were followed by MCF-7 cells. DOX-loaded composite nanoparticles and free DOX (final DOX concentration: 1 μg/mL) were incubated in MCF-7 culture at 37 °C for 0.5 and 2 h. The culture media were removed, and the cells were rinsed two times with PBS prior to the fluorescence observation.

2.6. Characterization Techniques. UV−vis spectra were obtained by a Perkin-Elmer Lambda 35 spectrophotometer. Fourier transform infrared (FT-IR) analysis was conducted on a Nicolet Nexus-440 FT-IR spectroscopy. The mesoporous channels were visualized using a FEI Tecnai F20 transmission electron microscope (HRTEM) operating at a voltage of 200 kV. The other products were performed on a JEOL 1230 transmission electron microscope (TEM) and TS 5136MM scanning electron microscopy (SEM). Core/shell composite nanoparticles were negatively stained with 1% phosphotungstic acid for TEM measurements. The size distribution of particles was measured by dynamic light scattering (DLS, autosizer 4700, Malvern). Zeta-potential was measured by a Zetasizer Nano-ZS (Malvern) at 25 °C. N_2 adsorption−desorption isotherms were obtained on a Micromeritics Tristar 3000 pore analyzer at 77 K under continuous adsorption conditions. Brunauer−Emmett−Teller (BET) and Barrett−Joyner−Halenda (BJH) analyses were used to calculate the surface area, pore size, and pore volume. Thermogravimetric analysis (TGA) was carried out on a Pyris 1 TGA thermal analyzer from 100 to 800 °C (10 °C/min) in a flow of N_2. MALDI-TOF mass spectrometry was performed on a Voyager DE-STR instrument. The cellular images were acquired with a confocal laser scanning microscope (CLSM, LEICA TCS SP5 II).

3. RESULTS AND DISCUSSION

3.1. Synthesis of Composite Nanoparticles. The overall synthetic scheme employed for the preparation of multifunctional core/shell composite nanoparticles, producing tunable thermo/pH-probing ability and a redox-responsive sheddable polymer shell wall, was illustrated in Scheme 1. High-quality of MSN seeds were synthesized by utilizing CTAB as template via base-catalyzed co-condensation of silicates.[25] Subsequently, CTAB-containing MSN was dispersed in anhydrous ethanol for the surface functionalization with a silane coupling agent of MPS, which generated a −C═C− MSN surface and in addition can afterwards react in the radical polymerization promoting PVCL network attachment to the MSN core.[28] In this exploration, nonacrylamide PVCL was chosen as a model system not only because its swelling and shrinking temperature is near the body temperature (37 °C) but also stems from its more biocompatibility than the most examined PNIPAM.[29] After that, the inserted CTAB template was removed to yield mesoporous channels. To offer efficient pH-responsible release kinetic deviated from our reported results,[27] superficially modified MSN channels with carboxylic acid was produced by a postsynthesis method. In the last part, a cross-linked polymer shell was prepared through precipitation polymerization of various monomers, including VCL, MAA, and BAC. Finally, for increasing the water dispensability in biomedical application, composite nanoparticles of MSN-COOH@P(VCL-*s*-*s*-MAA) were immediately PEGylated in a one-pot system to block the binding of proteins and minimize

dx.doi.org/10.1021/cm3037197 | *Chem. Mater.* 2013, 25, 574−585

nanoparticles aggregation.[30] The main idea behind this PEGylated approach was to spatially confine the presence of free PEG chains at the outermost surface of core/shell composite nanoparticles. It was highly requisite in preventing the interference of hydrophilic component in the phase transition of PVCL.

Figure 1 demonstrated the morphology and structural evolution of the synthesis products. The obtained colloidal

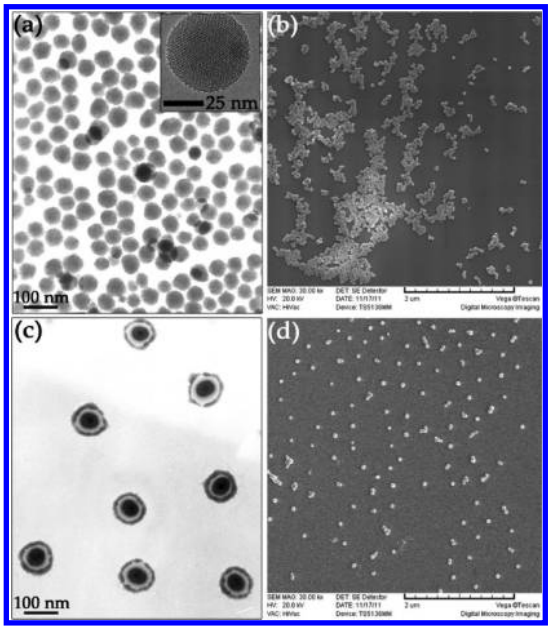

Figure 1. TEM and SEM images of MSN (a, b) and MSN-COOH@P(VCL-*s*-*s*-MAA)-PEG (c, d). Inset showed a typical HRTEM image of MSN. The dark ring in TEM image of (c) was obtained by stained phosphotungstic acid to enhance the polymer shell contrast.

MSN had a uniform, discrete spherical shape with an average diameter of 50 ± 10 nm (Figure 1a, b) by manually measuring over 100 particles, and well-ordered mesopores were also displayed obviously (the inset of Figure 1a). The regular MSN core resulted in a narrow size distribution of the final composite nanoparticles, which could be clearly dictated from TEM and SEM images (Figure 1c, d). Furthermore, the resultant hybrid MSN-COOH@P(VCL-*s*-*s*-MAA)-PEG composite nanoparticles showed individual separation from one another on the substrate in comparison to the native MSN, which was fully certificated that the polymer shell of P(VCL-*s*-*s*-MAA)-PEG indeed coated on MSN seeds. Intriguingly, the core/shell structure was significantly displayed (Figure 1c), with a single core of MSN (gray core) directly in the center of the polymer shell (bright ring). The average diameter of MSN-COOH@P(VCL-*s*-*s*-MAA)-PEG was about 70 nm with a standard deviation of 5 nm. Additionally, the DLS measurement also indicated that the hydrodynamic diameter increased upon completion of a coating polymer shell: 60 nm for the MSN core and 120 nm for MSN-COOH@P(VCL-*s*-*s*-MAA)-PEG at 55 °C in a collapsed polymer shell state. It was worth mentioning that both the specimens had a low size polydispersity index (<0.1) and were stable for several months. The significant diversity in the DLS diameters unequivocally confirmed the presence of a polymer shell. The hydrodynamic diameter measured by DLS was larger than the particle size presented in the corresponding TEM images because of the hydrate layer in an aqueous environment.[31] The comparison between DLS and TEM data suggested that the polymer coating procedure avoided agglomeration of nanoparticles into the larger aggregates.

For the preparation of core/shell composite nanoparticles with P(VCL-*s*-*s*-MAA)-PEG gatekeepers described in Scheme 1, a series of surface functionalization was monitored using FT-IR (Figure 2a). Concomitant with removal of the CTAB

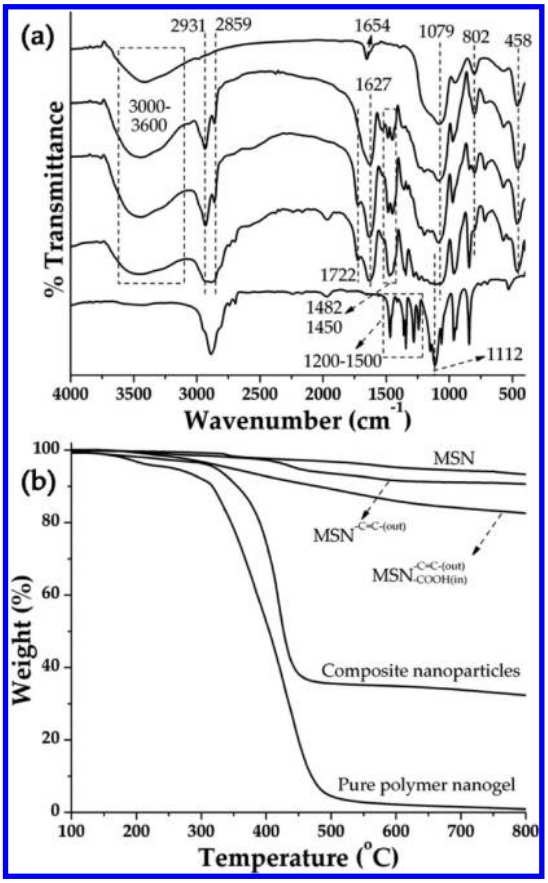

Figure 2. Characterization of MSN before and after polymer coating procedure: (a) FT-IR of MSN, MSN-COOH@PVCL, MSN-COOH@P(VCL-*s*-*s*-MAA), MSN-COOH@P(VCL-*s*-*s*-MAA)-PEG and PEG (from up to down); (b) TGA of samples described in the text.

surfactant, a strong intensity for water bending vibration at 1654 cm^{-1} was observed for MSN, which was ascribed to a hydrophilic silanol surface after template extraction.[32] The successful grafting of MPS onto the MSN surface was validated by the appearance of a C═O stretching band at 1720 cm^{-1} and $-CH_2$ stretching at 2958 cm^{-1}. Other IR bands that corresponded to $MSN^{-C=C-(out)}$ were similar to that of MSN due to the low MPS grafting density, so its spectroscopy was not deliberately shown. According to the synthetic version of as-prepared composite nanoparticles with three altered coating walls, PVCL, P(VCL-*s*-*s*-MAA), and P(VCL-*s*-*s*-MAA)-PEG, several vibration peaks at 1627 cm^{-1} of amide I band and 1482 cm^{-1} of C−N belonged to the characteristic peaks of PVCL.[33] The bands appearing at 2931, 2859, and 1450 cm^{-1} were attributed to stretching and bending vibrations of C−H groups, respectively.[34] These estimates can be a proof that the polymer shell had been successfully linked to the MSN core in combination with the TEM image of a bright ring. In addition,

dx.doi.org/10.1021/cm3037197 | *Chem. Mater.* 2013, 25, 574−585

MSN silica framework of composite nanoparticles remained unchanged upon polymer coating, as shown by the preservation of peaks at 458, 802, and 1079 cm^{-1}.[35] It should be noted that the shoulder peak of C═O stretching for carboxylic acid was also observed at 1722 cm^{-1} for MSN-COOH@P(VCL-*s*-*s*-MAA), confirming the successful copolymerization of VCL and MAA.[36] As the feed mass ratio of MAA/VCL increased, the intensity of the shoulder peak increased apparently, construing that the MAA content in the P(VCL-*s*-*s*-MAA)-PEG shell could be easily regulated. The polymer coated MSN composite nanoparticles were synthesized by seed precipitation polymerization in a batch reactor following a two-stage strategy, which consisted of placing VCL, MAA, and BAC at the beginning and adding a shot of a fixed amount of PEG-MA solution into the above mixture after 30 min of reaction. The available structure for MSN-based nanocomposites would be comprised of the P(VCL-*s*-*s*-MAA)-rich wall and near-surface corona grafting of PEG chains.[37] To further verify PEGylation of MSN-COOH@P(VCL-*s*-*s*-MAA), FT-IR analysis of composite nanoparticles was done, and pure PEG was used as control. C−O−C stretching vibration at 1112 cm^{-1} and C−H, N−H bending vibrations from 1200 to 1500 cm^{-1} can also be observed on the spectrum of MSN-COOH@ P(VCL-*s*-*s*-MAA)-PEG.[38] The result brought out the fact that PEG chains were successfully fixed on the peripheral surface of P(VCL-*s*-*s*-MAA) wall by covalent bonding after the radical copolymerization. Quantitative assessment of the organic content was also executed by means of TGA from 100 to 800 °C under N_2 atm (Figure 2b). No notable weight decrease could be observed for blank MSN in the tested temperature range except a lower weight loss (less than 6 wt %) above 600 °C, originating from the dehydroxylation of silanol.[39] In the case of as-prepared silanes modified MSN, a weight loss of 2.7 wt % and 8.0 wt % was due to the decomposition of organic functional groups of $MSN^{-C=C-(out)}$ and $MSN^{-C=C-(out)}_{-COOH(in)}$, respectively. It was found that pure PVCL nanogels underwent a main decomposition in the range of 300−500 °C, and its weight reached to zero at 800 °C.[33] After the seeds precipitation polymerization for hybrid composite nanoparticles, however, a remarkable loss in weight was found in the same temperature region, as evidenced from the weight loss in Figure 2b. Using the $MSN^{-C=C-(out)}_{-COOH(in)}$ core as a reference, the weight fraction of a cross-linked polymer outside of MSN-COOH@P(VCL-*s*-*s*-MAA)-PEG nanoparticles was about 50.3 wt %, which was consistent very well with the FT-IR analysis.

As shown in Figure 3 and Table 1, one can found that both N_2 adsorption−desorption isotherms for MSN and MSN-COOH@P(VCL-*s*-*s*-MAA)-PEG depicted the typical IV behavior for a well-developed mesostructure according to IUPAC, with a sharp adsorption step at 0.1−0.3 relative pressure (P/P0) range. An adsorption proceeded via multilayer adsorption, followed by an increase of capillary condensation.[40] The secondary adsorption step (P/P0 ~0.95) was attributed to interspace formed among the designed nanoparticles after freeze-drying. In addition, the capillary condensation evaporation in mesopores was reversible, so there were narrow or no type-H1 hysteresis loops in the isotherms. In the case of MSN-COOH@P(VCL-*s*-*s*-MAA)-PEG, the adsorption step was not so steep compared with MSN seeds, and the inflection point of step shifted to somewhat lower P/P0, suggesting a little reduction both in the pore diameter (inset of Figure 3) and the uniformity of MSN channel size, which can be subsequently illustrated by the pore structure parameters calculated from the

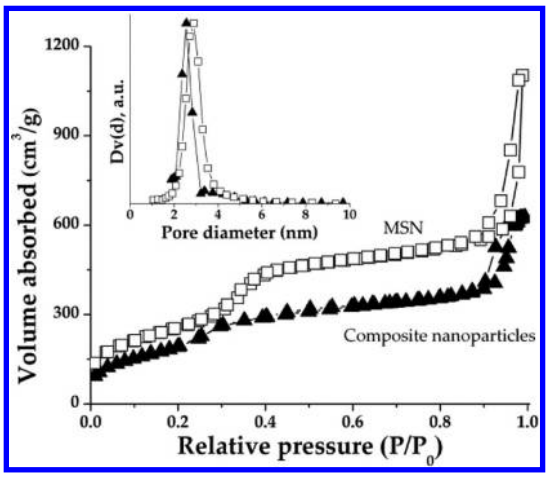

Figure 3. N_2 adsorption−desorption isotherms (inset: pore diameter distribution) for MSN before and after coating the polymer shell.

Table 1. N_2 Adsorption−Desorption Results of Samples Described in the Text

samples	surface area (m^2/g)[a]	pore volume (cm^3/g)	pore diameter (nm)[b]
MSN	950	1.7	2.9
$MSN^{-C=C-(out)}$	930	1.7	2.9
$MSN^{-C=C-(out)}_{-COOH(in)}$	910	1.5	2.8
MSN-COOH@P(VCL-*s*-*s*-MAA)-PEG	840	1.3	2.7

[a]BET specific surface area. [b]Pore diameter was calculated with the BJH method from the desorption branch.

adsorption branch (Table 1). For instance, the surface area, pore volume, and pore diameter of MSN were 950 m^2/g, 1.7 cm^3/g, and 2.9 nm, respectively. Actually, after being coated with P(VCL-*s*-*s*-MAA)-PEG, these parameters were 840 m^2/g, 1.3 cm^3/g, and 2.7 nm, respectively. The surface area and pore volume declined steadily, while pore diameter remained essentially identical after inclusion of the polymer shell, giving a direct evidence that P(VCL-*s*-*s*-MAA)-PEG was introduced and distributed predominantly on the exterior surface of the MSN core. As expected, MSN-COOH@P(VCL-*s*-*s*-MAA)-PEG composite nanoparticles with the retained mesoporosity had potential developments in the area of a stimulus-responsive release platform filled with an anticancer drug for the tumor therapy. This point will be discussed exhaustively below.

As seen in Table 1, the BET mesostructural parameters for MSN modified with MPS and −COOH were very similar to that of the nonfunctionalized MSN core. To avoid the overlap of BET isotherms, only two representative curves for MSN before and after coating the polymer were shown in Figure 3. Samples with higher weight loss in TGA had smaller surface area and pore diameter correspondingly. No pore diameter reduction for $MSN^{-C=C-(out)}$ proved that MPS groups were exclusively placed at the external surface of MSN. This observation could be further applicable to conclude that by performing the postgrafting of template-filled MSN, diffusion of silane coupling reactant into the porous structure was limited,[41] thus leading to a preferential functionalization of outer MSN surface. Significantly, the surface area and pore volume of $MSN^{-C=C-(out)}_{-COOH(in)}$ were reduced to 910 m^2/g and 1.5 cm^3/g, respectively. However, a minor reduction of pore diameter was observed. Discrete organic groups cannot obviously influence

dx.doi.org/10.1021/cm3037197 | *Chem. Mater.* 2013, 25, 574−585

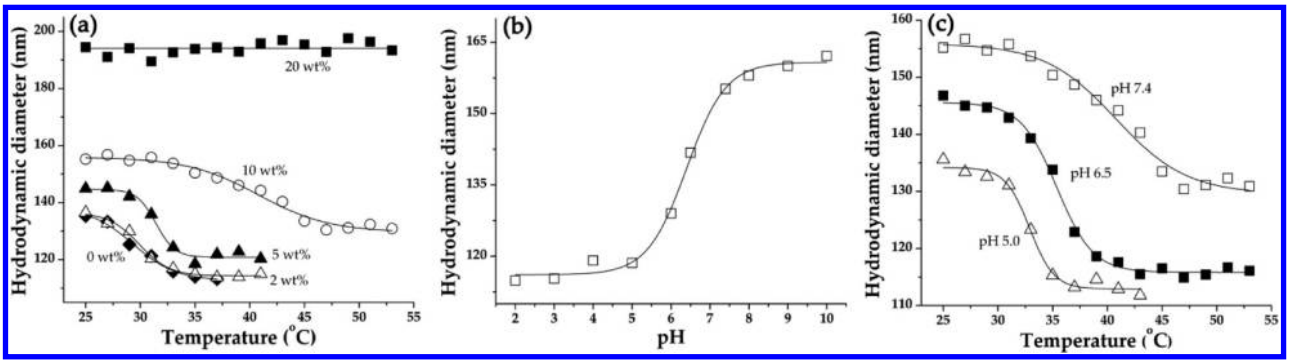

Figure 4. Thermo/pH-response of composite nanoparticles in 0.15 M NaCl solution. (a) Effect of MAA content on temperature dependence of hydrodynamic diameter of MSN-COOH@P(VCL-*s*-*s*-MAA)-PEG/X at pH 7.4. Legend for MAA content X: (■) 20 wt %, (○) 10 wt %, (▲) 5 wt %, (△) 2 wt %, (♦) 0 wt %. (b) pH dependence of hydrodynamic diameter of MSN-COOH@P(VCL-*s*-*s*-MAA)-PEG/10 at 25 °C. (c) Effect of pH on temperature dependence of hydrodynamic diameter of MSN-COOH@P(VCL-*s*-*s*-MAA)-PEG/10 at (□) pH 7.4, (■) pH 6.5, and (△) pH 5.0.

pore size due to their small concentration on channel walls. In general terms, it was convenient to have the choice of hosting large amounts of pharmaceuticals into the carrier matrix.

3.2. Thermo/pH-Sensitive Behaviors. Most of the intelligent polymers have been focused on thermo and pH responsive polymeric systems, because these are two important environmental factors in the body, and some disease states manifest themselves by a change in temperature and/or pH.[1] The volume phase transition of stimuli-sensitive polymers, such as PNIPAM and PVCL, as well as the swelling/deswelling degrees can be easily mediated by adjusting the composition of copolymer segments.[42] In this instance, it is known that a hydrophilic comonomer tends to increase the VPTT of microgel, while a hydrophobic comonomer displays the opposite trend. Versatile functional groups had been added to polymer chains by postpolymerization modification, thereby giving multifunctional polymers. In our experiments, the polymer shell was obtained by copolymerization of VCL and MAA, which are both temperature and pH sensitive.

The volume phase transition behavior of MSN-COOH@P(VCL-*s*-*s*-MAA)-PEG could be proved by DLS. In Figure 4a, the effect of the MAA content on thermosensitive volume phase transition of MSN-COOH@P(VCL-*s*-*s*-MAA)-PEG/X (X: MAA content in recipes) at pH 7.4 in 0.15 M NaCl suspension was assessed. In the synthesis route of composite nanoparticles, the cross-linker density (C_{BAC} = 10.0 wt %) and the concentration of KPS (0.1 mg/mL) were constant for all samples. DLS results showed a decrease in hydrodynamic diameters with an increase of temperature, corresponding to a volume phase transition. The temperature at which this phase separation occurs is called volume phase transition temperature (VPTT).[42] Obviously, as the increase of MAA content in MSN-COOH@P(VCL-*s*-*s*-MAA)-PEG, the hydrodynamic diameter increased greatly at a fixed temperature. In addition, some steep fall of deswelling fashion were observed when temperatures were close to critical VPTT values, shifted from 30.5 to 40.5 °C. It should be noted that the hydrodynamic diameter of MSN-COOH@P(VCL-*s*-*s*-MAA)-PEG/20 revealed a minor dependence on temperature, and no volume phase transition was presented in the studied temperature range (25−55 °C). After pH exceeded the p*K*a of MAA monomer (*ca.* 4.6),[43] MSN-COOH@P(VCL-*s*-*s*-MAA)-PEG nanoparticles began to expand due to osmotic swelling as well as electrostatic repulsion between the deprotonated carboxylic acid ($-COO^-$) groups. Thus at pH 7.4, the hydrophilicity and electrostatic repulsion of polymer segments increased when MAA contents increased. A volume phase transition would happen as soon as the balance factor of repulsive and hydrophobic force was accomplished. Higher incubation temperature was necessary to drive the disruption of hydrogen bond strengthened by increasing hydrophilicity.

The interactions between hydrophobic groups in response to temperature changes could not easily overwhelm the strong repulsion of $-COO^-$ units.[44] Therefore, with increasing MAA content, a higher temperature was required to cross this balance and allow volume phase transition.

Unless otherwise specified, MSN-COOH@P(VCL-*s*-*s*-MAA)-PEG/10 with MAA content of 10 wt % was selected in the subsequent research, because it presented the optimal morphology and highly feasible VPTT close to normal body temperature (Figure 4a). The hydrodynamic diameter of MSN-COOH@P(VCL-*s*-*s*-MAA)-PEG composite nanoparticles as a function of pH ranged from 2 to 10, at 25 °C with 0.15 M NaCl, was performed in Figure 4b. Obviously, the higher the pH value, the stronger the repulsive electrostatic forces and the larger the hydrodynamic diameter was obtained. The size of composite nanoparticles changed from 115 nm at pH 2 to 160 nm at pH 10. Importantly, the diameter of composite nanoparticles measured increased steeply when increasing pH from 4.0 to 7.0, bestowing remarkable pH sensitivity. This could be ascribed to the enhanced ionization degree of MSN-COOH@P(VCL-*s*-*s*-MAA)-PEG/10 with the increase of pH value. The coating polymer wall, P(VCL-*s*-*s*-MAA)-PEG/10 containing weakly acidic pendant MAA groups, was expected to exhibit pH responsiveness due to the alteration of the $-COOH/-COO^-$ ratio as the pH changes. $-COO^-$ groups were protonated at low pH; therefore, less charge repulsion occurred within the network, leading to the small size. The maximum swelling of composite nanoparticles nearly remained unchanged in a maximum degree of ionization around pH 8−10.[45] In this regard, the combination force of electrostatic repulsion compensated by hydrophobic force from copolymer chains was decreased with an increase of pH value, which induced a lower temperature to induce the phase transition of polymer shell.

To scrutinize the temperature and pH sensitivity of the core/shell composite nanoparticles, the influence of pH on VPTT of MSN-COOH@P(VCL-*s*-*s*-MAA)-PEG/10 was investigated at 0.15 M NaCl (Figure 4c). Composite nanoparticles at different pH displayed a similar evolution of hydrodynamic diameters as a function external temperature. For the case of pH 5.0, along with the increase of temperature, hydrodynamic diameters of

dx.doi.org/10.1021/cm3037197 | *Chem. Mater.* 2013, 25, 574−585

MSN-COOH@ P(VCL-*s*-*s*-MAA)-PEG/10 latex were gradually declined. Especially at lower or higher temperature, the diameter reduced slowly, but in a particular temperature range, the diameter changed with a sharp drop. It was clear that with pH increasing at a fixed temperature, the diameter of MSN-COOH@P(VCL-*s*-*s*-MAA)-PEG/10 increased significantly. These results represented that the pH value had a great effect on VPTT and varied in a narrow practical range. Concomitant with a pH reduction, the volume phase transition occurred at lower temperature, the VPTT of 40.5, 35.5, and 32.0 °C indexed to pH 7.4, 6.5, and 5.0, which was above, near, and below physiological temperature, respectively. This observation can be explained by a lower charge density existing in the network of P(VCL-*s*-*s*-MAA)-PEG/10 due to the deionization of carboxylic acid groups along with the decrease of pH, which resulted in electrostatic repulsion/hydrophobicity change of the copolymer shell.[46] The pH value varied in the range of 2−10 could effectively concentrate $-COO^-$ groups inside polymer networks. Principally, another key consequence might also be considered. Despite MAA being a water-soluble monomer, PMAA at lower pH is in a highly hydrophobic compact conformation.[47] While more −COOH groups fully deprotonated as pH rose, a hydrophobic−hydrophilic transformation was expected; that is when the environment changed from acidic to weak basic. Such a pH driven transformation was also anticipated to be reversible. Thus, this hydrophobic−hydrophilic balance of PMAA under pH control was attributed to the extra swelling extent and the shift of transition temperature of MSN-COOH@P(VCL-*s*-*s*-MAA)-PEG composite nanoparticles.

In principle, the criteria for thermo/pH-sensitive composite nanoparticles applied as the potential drug delivery systems were that the P(VCL-*co*-MAA) polymer shell can experience a distinct transition around a minor disturbance of human environment: a fully swollen state in the bloodstream after intravenous injection while a quickly collapsed state in tumor tissues. In this sense, no premature drug was penetrated from drug carrier whist having a rapid release upon reaching the tumor sites.[24] As clearly seen in Figure 4c, the MAA content of 10 wt % in a P(VCL-*s*-*s*-MAA) shell was undoubtedly conformed to control the release in a suitable kinetics. The thermo/pH/reduction-sensitive polymer wall had advantages for specific drug delivery application, depending on a variety of unique characteristics: tunable permeability and thickness, smart chemical composition and structure integrity, and nonspecific binding for prolonged circulation. Of equal importance in choosing drug storage was guided to the ability to encapsulate a vast amount of chemical drugs. Thus, composite nanoparticles of MSN-COOH@P(VCL-*s*-*s*-MAA)-PEG were chosen as the carrier of DOX, and the drug loading and release properties would be discussed.

3.3. The Role of Cross-Linker and Reductively Sheddable Behaviors. The aim of our work was to develop a novel MSN-based drug platform that contained reductively disrupted disulfide-cross-linked polymer shells for triggered controllable drug release. So far, it was still unclear whether the cross-linker of BAC indeed played a key role in the formation of a P(VCL-*s*-*s*-MAA) shell during the seed precipitation polymerization process. To answer this question, blank P(VCL-*s*-*s*-MAA)-PEG/10 nanogels were prepared by a surfactant-free emulsion polymerization analogous to that of the synthetic method for composite nanoparticles.[48] There was only one difference: no MSN core was used. The experimental phenomenon was monitored to confirm the effect of BAC amounts on the formation of P(VCL-*s*-*s*-MAA)-PEG/10 nanogels (Figure 5a)

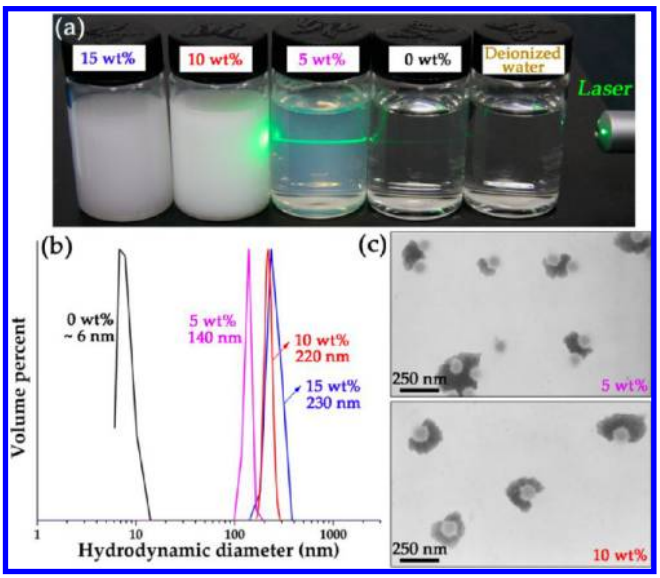

Figure 5. (a) Appearances of blank P(VCL-*s*-*s*-MAA)-PEG nanogel with various BAC cross-linking density: deionized water (a control set), 0, 5, 10, and 20 wt % (from right to left); (b) Effect BAC cross-linking density on the size distribution of blank P(VCL-*s*-*s*-MAA)-PEG at pH 7.4. (c) Typical TEM images of blank P(VCL-*s*-*s*-MAA)-PEG with 5 wt % and 10 wt % BAC cross-linking density. The dark ring in the TEM image was obtained by stained phosphotungstic acid to enhance the polymer contrast.

and then investigated by DLS and TEM (Figure 5b, c), respectively. First, a worthwhile control of deionized water was included in the experiment. A discrepancy in the feature of obtained emulsion was exceptionally distinct. The system without any cross-linker was a clear appearance similar to deionized water, and P(VCL-*s*-*s*-MAA)-PEG/10 nanogels with cross-linking density of 5 wt % was depicted completely light blue opalescent and formed a homogeneous stable nanosized latex at room temperature, as indicated by the perceptible "Tyndall effect" using a laser pointer aimed at the nanogel. While the latex size reaches the wavelength of visible light, emulsion will appear increasingly translucent and blue in color.[49] When the BAC amount in the recipe was elevated to 10 wt % and 20 wt %, it was interesting to note that pure nanogels with higher cross-linked densities became absolute opaqueness and white. Thus, it can be intuitively inferred that P(VCL-*s*-*s*-MAA)-PEG/10 nanogels with high cross-linker density were usually higher in the consideration of their total size. Accurate calculation of this trend for size change exposed to NaCl-free and pH 7.4 solutions had been followed by DLS. Notably, fast size enhancement was observed for P(VCL-*s*-*s*-MAA)-PEG/10 pure nanogels, where the hydrodynamic diameter of nanogel increased from about 6 nm for 0 wt % of BAC to 140 nm for 5 wt % of BAC, reaching over 200 nm above 10 wt % of BAC (Figure 5b). The approach featured the formation of linear polymer chain first (0 wt % of BAC) and then generated a cross-linked and tight nanogels by the BAC cross-linker. Using such batch radical polymerization, narrowly distributed nanogel was rapidly obtained (Figure 5c), which was discerned in typical TEM images for P(VCL-*s*-*s*-MAA)-PEG/10 with 5 wt % and 10 wt % of cross-linker density, respectively. The largely improved nanogel sizes strongly indicated the cross-linker had a

dx.doi.org/10.1021/cm3037197 | *Chem. Mater.* 2013, 25, 574−585

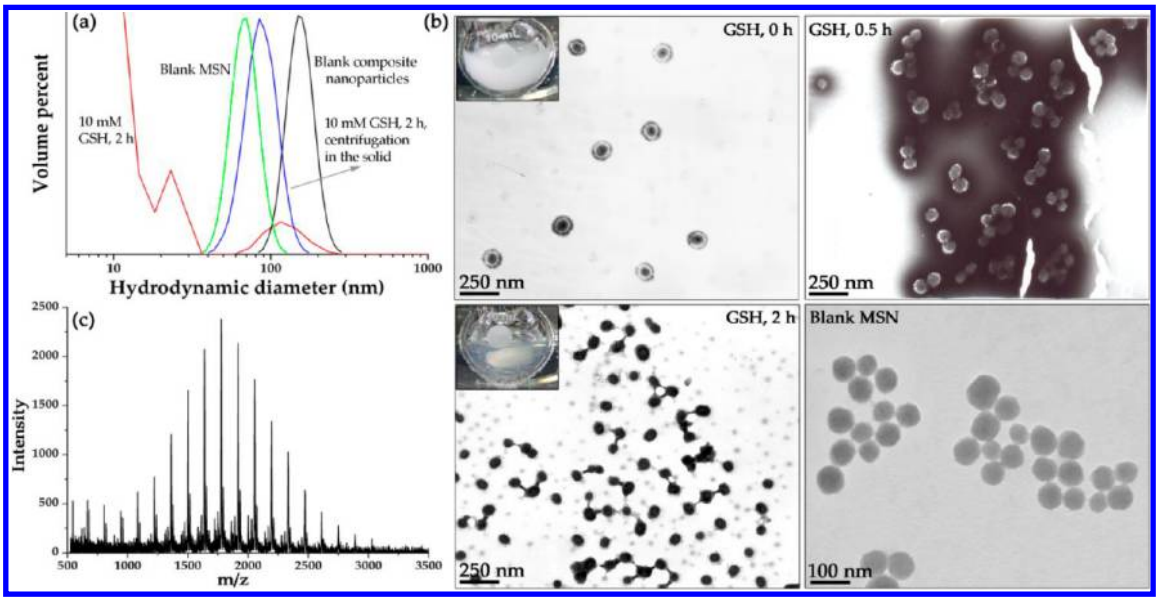

Figure 6. Reduction-sensitive MSN-COOH@P(VCL-*s*-*s*-MAA)-PEG (pH 7.4, 0.15 M NaCl). (a) Hydrodynamic diameter change determined in response to 10 mM GSH at 25 °C. (b) TEM images captured at different incubation times: 0, 0.5, and 2 h at 10 mM GSH. Inset: appearances at 0 and 2 h, respectively. (c) MALDI-TOF of the sheddable polymer chains after cleavage of disulfide bonds by GSH. To avoid influence from PEG molecular weight, MSNs-COOH@P(VCL-*s*-*s*-MAA) without PEG was synthesized.

marked and drastic effect on latex formation. The increase of the cross-linker amount in the batch polymerization recipe leads to a reduction in the final amount of water-soluble polymer.[50] It was necessary in the polymerization recipe to favor particle formation by cross-linking the precipitated P(VCL-*s*-*s*-MAA) polymer segments leading to generate the nucleation step. To maintain a nanogel structure rather than resoluble polymer chains, the BAC cross-linker was requisite to favor cross-linking efficiency of precipitated polymer chains under the nanogel state. In this perspective, the aforementioned analysis stage of qualitative and quantitative information on P(VCL-*s*-*s*-MAA)-PEG/10 nanogels implied that the cross-linked polymer wall using disulfides had a particular and considerable action in the preparation of core/shell structured MSN-COOH@ P(VCL-*s*-*s*-MAA)-PEG/10 composite nanoparticles.

The biomedical application of drug delivery systems including MSN materials is currently limited because of the instability and/or premature release of anticancer drugs upon administration.[51] In this work, the MSN core was coated with a multisensitive P(VCL-*s*-*s*-MAA)-PEG shell cross-linked by disulfides to yield a sheddable polymer wall, which was supposed to be stable in circulation but rapidly de-cross-linked in a reductive environment such as cytoplasm. The reduction-responsiveness of P(VCL-*s*-*s*-MAA)-PEG was studied in great detail, which gave specific insight for understanding the sheddable evolution of the polymer wall. The size change of MSN-COOH@P(VCL-*s*-*s*-MAA)-PEG composite nanoparticles exposed to 10 mM reductant GSH buffer (0.15 M, pH 7.4) was explored using DLS and TEM, in order to investigate whether the P(VCL-*s*-*s*-MAA)-PEG/10 shell outside of the MSN-COOH core could break away. In line with our expectations, environment conditions had a great influence on the size and quality (PDI) of the obtained composite nanoparticles (Figure 6a). When incubating time increased to 2 h, the PDI of MSN-COOH@P(VCL-*s*-*s*-MAA)-PEG nanocomposites increased from 0.02 to 0.5 and hydrodynamic size decreased from a constant value (150 nm) to a fluctuating range. The polymer shell was rapidly dissociated to soluble chains with a size of 10−25 nm at 25 °C, whereas the MSN core allowed a weak volume intensity of scattering signal with its peak centered at 110 nm. These dissolved components of polymer chains could be easily removed by centrifugation, and the resulting isolation in solid state was redispersed in buffer. In contrast, the average size remarkably declined to 90 nm due to the reductive disintegration of intermediate disulfide chemical bonds,[52,53] which resulted in the shedding of the P(VCL-*s*-*s*-MAA)-PEG/10 shell. Notably, only slightly changes in size distribution belonging to the core part occurred with respect to virgin MSN as a reference. Moreover, TEM images in Figure 6b also offered strong evidence that MSN-COOH@P(VCL-*s*-*s*-MAA)-PEG composite nanoparticles possessed reduction sensitivity. The striking contrast between the MSN core and the shell part was enhanced by the settlement of phosphotungstic acid attached to the polymer wall edge, and TEM observations clearly showed that the thickness of the P(VCL-*s*-*s*-MAA)-PEG shell (bright ring) led to a reduced tendency over the studied degradation period. A comparison of TEM results highlighted the impact of GSH on polymer shell erosion following BAC cleavage. In the extreme case of adding GSH after 2 h, most likely, complete dissolution for the polymer shell was observed, and composite nanoparticles were directly turned into the MSN core alone. Together, those data suggested that the cross-linking reaction took place exclusively within the P(VCL-*s*-*s*-MAA)-PEG polymer shell network. Under the simulated intracellular reducing conditions, the rupture of periphery for composite nanoparticles caused a totally degradable polymer shell, which in turn decreased its total shell wall thickness as well as facilitated an enhanced drug releasing activity. MSN-COOH@P(VCL-*s*-*s*-MAA)-PEG/10 composite nanoparticles with a reductively sheddable polymer shell gate, whose integrity of polymer network was totally tuned by the disulfide cross-linkers, were supposed to own crucial importance in the tailored release fashion. The molecular weight of the composite nanoparticles-associated polymer chain (M_w) after the sheddable P(VCL-*s*-*s*-MAA) wall was charac-

dx.doi.org/10.1021/cm3037197 | *Chem. Mater.* 2013, 25, 574−585

terized by MALDI-TOF mass spectra (Figure 6c). In order to avoid M_w influence from PEG, new composite nanoparticles without the addition of PEG-MA in the recipe was synthesized. Normally, the accumulation of the nondegradable polymer occurred when it used a M_w greater than the renal threshold.[54] It is more acceptable that polymer M_w below 30000 g/mol is optimized to ensure ultimate renal elimination at the same time as allowing tumor targeting. The M_w of removal polymer chain after cleavage of the disulfide bond showed approximately 1800 g/mol, which provided considerable and paramount evidence to imply the potential usage of the synthesized composite nanoparticles as a drug delivery system by intravenous route without leaving any toxic byproducts.

3.4. *In Vitro* Drug Release and Cell Assay. DOX is one of the most potent anticancer drugs and is widely used in the treatment of various types of solid malignant tumors by interacting with DNA via intercalation.[55] However, the life-threatening side effect for DOX-based therapy is cardiotoxicity. It is crucial, therefore, to deliver and release DOX in cytoplasm and right into the cell nucleus. The aim of our work was to develop a triggered intracellular delivery system for DOX, which may lead to enhanced cancer chemotherapy. The incorporation of DOX was commonly loaded by soaking MSN-COOH@P(VCL-*s*-*s*-MAA)-PEG nanoparticles in a highly concentrated drug solution at pH 8.5 for 12 h, and magnetic stirring should be applied to favor the diffusion of drug molecules into mesopores. The theoretical drug loading content was set at a mass ratio of 0.3 between DOX and composite nanoparticles. The actual drug loading content was about 21.5 wt % under alkaline conditions of pH 8.5. The DOX loading process predominantly relied on a physical adsorption mechanism in mesoporous channels. Near the isoelectric point of DOX (8.5−9.0),[56] the net charge of DOX molecules were around zero. Thus, electrostatic attractions between the polymer shell and drug molecules were minimal. Meanwhile, as the elevated electrostatic repulsion was provided by deprotonated −COOH groups at a higher pH, DOX would easily absorb into MSN channels across the relatively large mesh size of the polymer shell. Thus, drugs packed densely on the adsorbent surface should be sequestered preferentially into composite nanoparticles via nonspecific hydrophobic partitioning,[57] as long as they can gain access to the interior cavities.

After confirmation that DOX had been stored into MSN-COOH@P(VCL-*s*-*s*-MAA)-PEG, a question instantaneously arose: were the drug molecules confined inside the MSN core part or were they just distributed in the P(VCL-*s*-*s*-MAA)-PEG polymer shell layer. This was the million dollar question for all researchers in this area. To solve it, several analytical techniques had been employed to find out what was going on inside carriers. First, GSH was introduced to a cuvette with 3 mL of DOX-loaded MSN-COOH@P(VCL-*s*-*s*-MAA)-PEG (pH 8.5), leading to a final 10 mM GSH concentration. The cuvette was sealed and placed at 37 °C for 1 h. Then it was isolated into two samples: centrifugal precipitate and supernatant. Initially, DOX-loaded composite nanoparticles acquired the more deep red appearance, but following centrifugation resulted in a reddish color of centrifugal precipitate and slight yellowish-red colored supernatant (Figure 7a). It is known that DOX is dissolved in water at low pH but insoluble in an alkaline solution above its isoelectric point. Therefore, a higher pH was adjusted to ensure the diffusion of DOX as little as possible. The BET surface area of the centrifugal precipitate was significantly decreased by 2 orders of magnitude (Figure 7b)

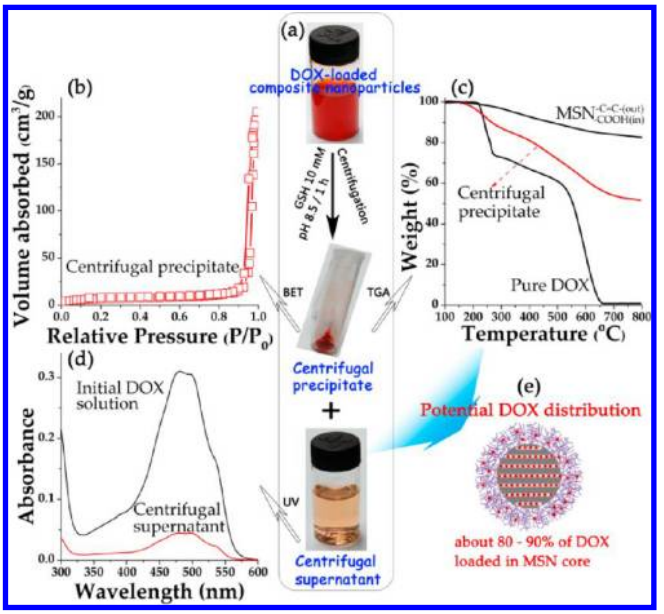

Figure 7. Characterization of the entrapped DOX location in MSN-COOH@P(VCL-*s*-*s*-MAA)-PEG. (a) Controlled centrifugal separation procedure of DOX-loaded composite nanoparticles after cleavage of disulfide bonds in the polymer shell by 10 mM GSH. Both the centrifugal precipitate and supernatant were collected, respectively. To minimize drug releasing from the MSN core, a short GSH incubation time of 1 h was adopted. (b) BET isotherm and (c) TGA of centrifugal precipitate. (d) UV−vis spectra of initial DOX solution and the residual DOX content in centrifugal supernatant. (e) Representative illustration of location of DOX loaded in composite nanoparticles.

compared to 910 m^2/g of MSN, giving a strong suggestion that DOX molecules loading in the MSN core part blocked the mesopores. The DOX amount in the centrifugal precipitate was 30.8 wt % by TGA (Figure 7c), which was about 81.5% of the total drug loading content (21.5 wt %) for composite nanoparticles when the weight fraction of the polymer shell of 50.3 wt % (Figure 2b) was considered. UV−vis absorbance also demonstrated the capability of DOX loading into the MSN domain (Figure 7d). It could be seen that the UV−vis curves coincided very well, but absorption intensity of centrifugal supernatant was more apparently decreased. As a result, the drug loading fraction in the MSN domain could reach up to 89 wt %. On the basis of these results, we confirmed that about 80−90% of DOX was filled into the MSN core (Figure 7e), that is, nearly most of the drug molecules were confined inside the mesoporous channels acting as a drug storage platform.

In view of the aforementioned discussions, the extended research was necessary to evaluate whether the elaborated thermo/pH and redox-sensitive P(VCL-*s*-*s*-MAA)-PEG/10 polymer shell had a regulation effect involved in the DOX release route. As shown in Figure 8, the drug release experiments were conducted at 37 °C and 0.15 NaCl concentrations in three simulated body fluids, i.e. pH 7.4 (below VPTT), pH 6.5 (at VPTT), and pH 5.0 (above VPTT). Regardless of the pH values, DOX-loaded carriers had a marked sustained release property. The drug delivery system consisting of P(VCL-*s*-*s*-MAA)-PEG coated MSN composite nanoparticles exhibited only 5.4% of drug release in pH 7.4 buffer over a period of 24 h. The detection construed a prominent capping efficiency of the polymer shell for encapsulation of DOX molecules against the undesired leaching problem. With the decline of pH in solution, the DOX release profile from

dx.doi.org/10.1021/cm3037197 | *Chem. Mater.* 2013, 25, 574−585

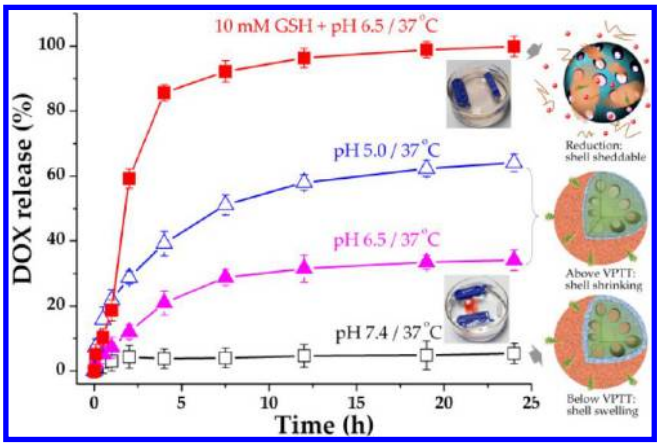

Figure 8. pH-dependent DOX release from DOX-loaded MSN-COOH@P(VCL-*s*-*s*-MAA)-PEG in 0.15 M NaCl solution at (□) pH 7.4, (▲) pH 6.5, (△) pH 5.0, and (■) pH 6.5 with 10 mM GSH. Inset: two releasing phenomena after 24 h. The right diagrams: three schematic releasing mechanisms.

MSN-COOH@P(VCL-*s*-*s*-MAA)-PEG in acidic conditions (pH 6.5 and 5.0) showed a relatively rapid release rate. After 24 h releasing, the amount of released DOX reached 34.1% for pH 6.5 and 64.2% for pH 5.0, respectively. As a comparison, the drug release experiment of pure DOX had been performed by the same procedure (data not shown), and DOX was totally released within 2 h both at pH 5.0 and 7.4. This result indicated that DOX can freely cross dialysis membrane, independent of the incubated pH. The significantly diversified DOX release events under altered pH intervention can be mainly attributed to the structural transitions (collapse or swelling, diagrams in Figure 8) of the P(VCL-*s*-*s*-MAA)-PEG polymer shell. It had been proved that the internal structure of thermo-sensitive microgels was loose and had high permeability,[58] allowing for drug molecules to be readily diffused from the interior of microgels in a rather easy way. DOX diffusion across the polymer shell had a distance-limiting mechanism.[24] With this regard, the polymer shell was in the swollen state at pH 7.4/37 °C, thereby impeding and retarding the diffusion capability of DOX. On the other hand, the enhanced electrostatic attraction among positively charged DOX molecules and the negatively charged MSN-COO^- core and polymer shell was unfavorable for the mass-transport of DOX molecules.[59] However, when pH decreased to 5.0, the polymer wall was collapsed due to the VPTT of composite nanoparticles less than 37 °C. As a consequence, the thinner shell corona and disrupted electrostatic interaction facilitated a fast DOX diffusion. Albeit significant acceleration of DOX releasing was observed upon adjusting pH to 5.0, the most rapid release rate was achieved when the dual stimuli of pH/thermo and GSH were utilized simultaneously. In the latter case, about 95% of DOX was released within just 12 h. This was in line with the previous observation that the polymer shell in MSN-COOH@P(VCL-*s*-*s*-MAA)-PEG was destabilized, and disintegration of the polymer wall was stimulated in response to GSH. It would be logical to assume that both reduction and thermo/pH stimulus contributed to the drug release efficiency. Besides, there was no contradiction among polymer shell-limiting, electrostatic and reductively sheddable mechanisms; apparently they complemented each other. The contribution of either mechanism depended on the external stimulus. No initial burst release was observed, and DOX releasing from MSN-COOH@P(VCL-*s*-*s*-MAA)-PEG composite nanoparticles was in a zero order manner up to 80% amount. The constant release rate indicated that release of DOX was tuned most likely by a combination of diffusion and shell-degradation. Therefore, shedding of the P(VCL-*s*-*s*-MAA) polymer wall represented a highly promising approach to achieve the capacity for near instantaneous controlled drug delivery.

The PEGylated multiresponsive MSN-COOH@P(VCL-*s*-*s*-MAA)-PEG is particularly useful in tumor-targeted drug delivery, which is known for increasing carrier circulation time by decreasing eticuloendothelial system clearance.[60] It is expected that DOX is sufficiently stable in composite nanoparticles with minimal drug leakage during the blood circulation. Then, upon reaching the targeted tumor tissues by EPR effect, rapid DOX release would be subject to certain enhancement. Subsequent contraction and shedding of the polymer shell can be accomplished in cytosol after cellular uptake,[61] with the subsequent release of the loaded DOX occurring at an apparently accelerated rate.

The releasing of DOX after the cellular uptake of DOX-loaded composite nanoparticles was evaluated by MCF-7 cancer cells via CLSM. For free DOX in 0.5 h, fluorescence was distributed in the surroundings of the cell nucleus (Figure 9a),

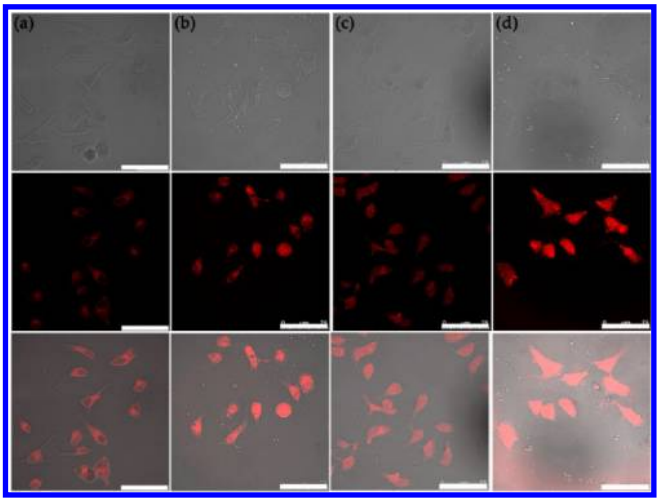

Figure 9. CLSM images of the intracellular DOX release from MSN-COOH@P(VCL-*s*-*s*-MAA)-PEG composite nanoparticles using MCF-7 cells. Free DOX was used as a control. (a) 0.5 h and (b) 2 h incubation of free DOX; (c) 0.5 h and (d) 2 h incubation of DOX-loaded composite nanoparticles. DOX concentration for both samples was 1 μg/mL. In each column, images from top to down: differential interference contrast microscopy, fluorescence microscopy, and overlays of both images. Scale bars correspond to 75 μm in all the images.

and, after 2 h, DOX was observed in the cell nucleus in addition to the significant fluorescence in cytoplasm (Figure 9b). In contrast, DOX-loaded composite nanoparticles efficiently delivered and released DOX into the nucleus for just only 0.5 h (Figure 9c), thus corroborating the fast shedding of the polymer shell inside cells. A longer incubation time of 2 h (Figure 9d) resulted in a stronger DOX fluorescence in the whole cell. The rapid release of DOX from MSN-COOH@P(VCL-*s*-*s*-MAA)-PEG inside cells was consistent with the data observed in the buffered solution (Figure 8). A comparably faster delivery of DOX into the cell nucleus using composite nanoparticles compared to free DOX was also reported by

dx.doi.org/10.1021/cm3037197 | *Chem. Mater.* 2013, 25, 574–585

Zhong et al.[62] The cell uptake of free DOX is a passive diffusion process, while for DOX-loaded nanoparticles, a possible endocytosis mechanism is involved,[63] which is more effective than the passive diffusion. Based on these results, the low pH and reducing agent in lysosomes could cause reductive cleavage of the polymer wall, thereby resulting in the rapid lysosomal release and nucleic accumulation of DOX anticancer drugs.

The careful investigation on the cytotoxicity of composite nanoparticles of MSN-COOH@P(VCL-*s*-*s*-MAA)-PEG also had been checked before being applied as an effective drug carrier for the therapeutic treatment of tumors. The *in vitro* cytotoxicity against 293 normal cells and MCF-7 cancer cells were investigated by MTT assay, respectively. As shown in Figure 10, the drug platforms of MSN-COOH@ P(VCL-*s*-*s*-MAA)-PEG composite nanoparticles showed nearly no cytotoxicity to MCF-7 cells even up to a high concentration of 500 μg/mL. Significant growth inhibition of MCF-7 cells was observed when the cells were treated with either the suspension of DOX-loaded composite nanoparticles or a solution of pure DOX in PBS (pH 7.4) at a higher DOX concentration. Only 16.7% cells remained viable at a DOX dosage of 1 μg/mL after incubation with DOX-loaded composite nanoparticles. More importantly, it was intriguing to note that the cytotoxicity of DOX-loaded MSN-COOH@P(VCL-*s*-*s*-MAA)-PEG composite nanoparticles was very similar to that of pure DOX, i.e. the IC50 value (the concentration of drugs required to reduce cell growth by 50%) was determined to be 0.09 and 0.07 μg/mL, respectively. Therefore, this DOX-loaded composite nanoparticle displayed high cytotoxicity with enough efficiency to kill the cancer cells.

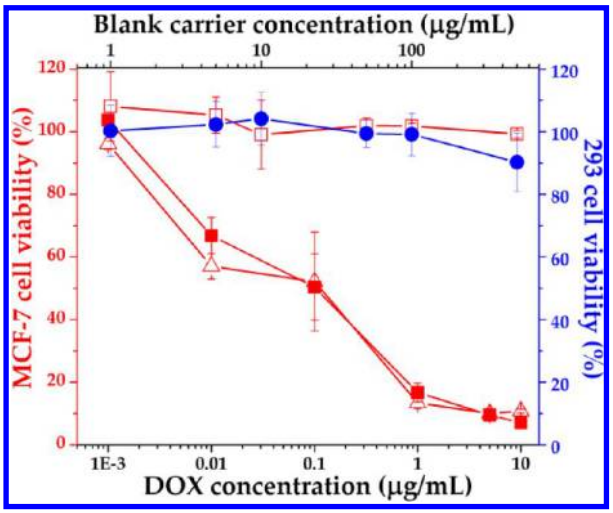

Figure 10. Cell survival assay. MCF-7 cancer cells (red): (□) MSN-COOH@P(VCL-*s*-*s*-MAA)-PEG, (■) DOX-loaded MSN-COOH@ P(VCL-*s*-*s*-MAA)-PEG and (Δ) free DOX. 293 normal cells (blue): (●) MSN-COOH@P(VCL-*s*-*s*-MAA)-PEG. The concentration of blank MSN-COOH@ P(VCL-*s*-*s*-MAA)-PEG was shown on the top *x*-axis.

For 293 normal cells (Figure 10), MSN-COOH@P(VCL-*s*-*s*-MAA)-PEG composite nanoparticles had a negligible reduction in the cell viability with increasing the concentration from 0.1 to 100 μg/mL, exhibiting a good biocompatibility for composite nanoparticles. However, an obvious decrease in cell viability of about 85% was kept at the concentration of 500 μg/mL, indicative of a certain degree of cytotoxicity at higher concentration. The result of cytotoxicity to 293 cells showed that MSN-COOH@ P(VCL-*s*-*s*-MAA)-PEG was a nontoxic material at low concentration and is suitable as a drug carrier.[8] It should be mentioned that the concentration of composite nanoparticles was too low to induce toxicity to normal cells, when utilized as a platform for anticancer drugs. It can foresee that these well-fabricated composite nanoparticles with multilayer structures are intriguing candidates for effective drug carriers in tumor therapy.

CONCLUSIONS

In this work, a proof of the novel concept of a bioresponsive controlled drug release nanocarrier was introduced, using the MSN-COOH core applied as the storage platform where entrapped high doses of therapeutic drugs, disulfide-cross-linked thermo/pH-sensitive and redox sheddable P(VCL-*s*-*s*-MAA)-PEG shell acted as gatekeepers. The estimates established that the phase state of the polymer coatings, including a variety of characteristics, thickness and permeability, chemical composition, and integrity, can open or close the entrance of mesoporous channels on command, so that the polymer shell was active in moderating the diffusion of embedded drugs in-and-out of the pore channels of MSN. Drug sequestration can be achieved in MSN core storage and significantly reduced in blood circulation, whereas a burst and total drug release was stimulated in an acidic and reductant-enriched environment such as the cytosol compartment which can disintegrate the gatekeeper by cleavage of the disulfide stalk moiety. Since no premature release in blood circulation and an accelerated drug release inside cancer cells are the two critical issues for conventional nanocarriers at present, the prepared core/shell structured composite nanoparticles of MSN-COOH@P(VCL-*s*-*s*-MAA)-PEG is extremely meaningful. *In vitro* cell assay revealed the great potential of the elaborated synergistic multisensitive composite nanoparticles for achieving an optimal and robust therapeutic effect of the transported drugs in cancer treatment.

AUTHOR INFORMATION

Corresponding Author

*E-mail: wlyang@fudan.edu.cn.

Notes

The authors declare no competing financial interest.

ACKNOWLEDGMENTS

We are grateful for the support of the National Science Foundation of China (Grant No. 20874015, 51273047) and the Shanghai Rising-Star Program (10QH1400200).

REFERENCES

(1) Schmaljohann, D. *Adv. Drug Delivery Rev.* **2006**, *58*, 1655−1670.
(2) Yiu, H. H. P.; Niu, H. J.; Biermans, E.; van Tendeloo, G.; Rosseinsky, M. J. *Adv. Funct. Mater.* **2010**, *20*, 1599−1609.
(3) Such, G. K.; Johnston, A. P. R.; Caruso, F. *Chem. Soc. Rev.* **2011**, *40*, 19−29.
(4) Poon, Z.; Chang, D.; Zhao, X. Y.; Hammond, P. T. *ACS Nano* **2011**, *5*, 4284−4292.
(5) Trewyn, B. G.; Slowing, I. I.; Giri, S.; Chen, H. T.; Lin, V. S. Y. *Acc. Chem. Res.* **2007**, *40*, 846−853.
(6) Lu, J.; Liong, M.; Li, Z. X.; Zink, J. I.; Tamanoi, F. *Small* **2010**, *6*, 1794−1805.
(7) Yamada, H.; Urata, C.; Aoyama, Y.; Osada, S.; Yamauchi, Y.; Kuroda, K. *Chem. Mater.* **2012**, *24*, 1462−1471.

(8) Manzano, M.; Vallet-Regi, M. *J. Mater. Chem.* **2010**, *20*, 5593−5604.
(9) Wang, Y. J.; Caruso, F. *Chem. Mater.* **2005**, *17*, 953−961.
(10) Wang, Y. J.; Yan, Y.; Cui, J. W.; Hosta-Rigau, L.; Heath, J. K.; Nice, E. C.; Caruso, F. *Adv. Mater.* **2010**, *22*, 4293−4297.
(11) Slowing, I. I.; Vivero-Escoto, J. L.; Wu, C. W.; Lin, V. S. Y. *Adv. Drug Delivery Rev.* **2008**, *60*, 1278−1288.
(12) Li, Z. X.; Barnes, J. C.; Bosoy, A.; Stoddart, J. F.; Zink, J. I. *Chem. Soc. Rev.* **2012**, *41*, 2590−2605.
(13) Luo, Z.; Cai, K. Y.; Hu, Y.; Zhao, L.; Liu, P.; Duan, L.; Yang, W. H. *Angew. Chem., Int. Ed.* **2011**, *50*, 640−643.
(14) Chen, C. E.; Geng, J.; Pu, F.; Yang, X. J.; Ren, J. S.; Qu, X. G. *Angew. Chem., Int. Ed.* **2011**, *50*, 882−886.
(15) Lai, C. Y.; Trewyn, B. G.; Jeftinija, D. M.; Jeftinija, K.; Xu, S.; Jeftinija, S.; Lin, V. S. Y. *J. Am. Chem. Soc.* **2003**, *125*, 4451−4459.
(16) Giri, S.; Trewyn, B. G.; Stellmaker, M. P.; Lin, V. S. Y. *Angew. Chem., Int. Ed.* **2005**, *44*, 5038−5044.
(17) Slowing, I. I.; Vivero-Escoto, J. L.; Trewyn, B. G.; Lin, V. S. Y. *J. Mater. Chem.* **2010**, *20*, 7924−7937.
(18) Torchilin, V. *Eur. J. Pharm. Biopharm.* **2009**, *71*, 431−444.
(19) Meng, F. H.; Hennink, W. E.; Zhong, Z. Y. *Biomaterials* **2009**, *30*, 2180−2198.
(20) Yang, Y.; Yan, X. H.; Cui, Y.; He, Q.; Li, D. X.; Wang, A. H.; Fei, J. B.; Li, J. B. *J. Mater. Chem.* **2008**, *18*, 5731−5737.
(21) Singh, N.; Karambelkar, A.; Gu, L.; Lin, K.; Miller, J. S.; Chen, C. S.; Sailor, M. J.; Bhatia, S. N. *J. Am. Chem. Soc.* **2011**, *133*, 19582−19585.
(22) Bhattacharyya, S.; Wang, H. S.; Ducheyne, P. *Acta Biomater.* **2012**, *8*, 3429−3435.
(23) Feng, P. Y.; Liu, R.; Liao, P. H.; Liu, J. K. *Langmuir* **2011**, *27*, 3095−3099.
(24) Chang, B. S.; Sha, X. Y.; Guo, J.; Jiao, Y. F.; Wang, C. C.; Yang, W. L. *J. Mater. Chem.* **2011**, *21*, 9239−9247.
(25) Lee, J. E.; Lee, N.; Kim, H.; Kim, J.; Choi, S. H.; Kim, J. H.; Kim, T.; Song, I. C.; Park, S. P.; Moon, W. K.; Hyeon, T. *J. Am. Chem. Soc.* **2010**, *132*, 552−557.
(26) Lang, N.; Tuel, A. *Chem. Mater.* **2004**, *16*, 1961−1966.
(27) Chang, B. S.; Guo, J.; Liu, C. Y.; Qian, J.; Yang, W. L. *J. Mater. Chem.* **2010**, *20*, 9941−9947.
(28) Karg, M.; Pastoriza-Santos, I.; Liz-Marzan, L. M.; Hellweg, T. *ChemPhysChem* **2006**, *7*, 2298−2301.
(29) Vihola, H.; Laukkanen, A.; Valtola, L.; Tenhu, H.; Hirvonen, J. *Biomaterials* **2005**, *26*, 3055−3064.
(30) Gong, J. L.; Pan, J.; Wan, D. *Chem. Commun.* **2011**, *47*, 3442−3444.
(31) Lapeyre, V.; Renaudie, N.; Dechezelles, J. F.; Saadaoui, H.; Ravaine, S.; Ravaine, V. *Langmuir* **2009**, *25*, 4659−4667.
(32) Moller, K.; Kobler, J.; Bein, T. *Adv. Funct. Mater.* **2007**, *17*, 605−612.
(33) Kozanoglu, S.; Ozdemir, T.; Usanmaz, A. *J. Macromol. Sci., Part A: Pure Appl. Chem.* **2011**, *48*, 467−477.
(34) Shah, S.; Pal, A.; Gude, R.; Devi, S. *Eur. Polym. J.* **2010**, *46*, 958−967.
(35) You, Y. Z.; Kalebaila, K. K.; Brock, S. L.; Oupicky, D. *Chem. Mater.* **2008**, *20*, 3354−3359.
(36) Yang, Q.; Wang, S. H.; Fan, P. W.; Wang, L. F.; Di, Y.; Lin, K. F.; Xiao, F. S. *Chem. Mater.* **2005**, *17*, 5999−6003.
(37) Imaz, A.; Forcada, J. *J. Polym. Sci., Part A: Polym. Chem.* **2011**, *49*, 3218−3227.
(38) Liu, J. S.; Xu, T. W.; Gong, M.; Yu, F.; Fu, Y. X. *J. Membr. Sci.* **2006**, *283*, 190−200.
(39) Kobler, J.; Moller, K.; Bein, T. *ACS Nano* **2008**, *2*, 791−799.
(40) Wu, K. C. W.; Chiang, Y. D.; Lian, H. Y.; Leo, S. Y.; Wang, S. G.; Yamauchi, Y. *J. Phys. Chem. C* **2011**, *115*, 13158−13165.
(41) Kecht, J.; Schlossbauer, A.; Bein, T. *Chem. Mater.* **2008**, *20*, 7207−7214.
(42) Nayak, S.; Lyon, L. A. *Angew. Chem., Int. Ed.* **2005**, *44*, 7686−7708.
(43) Saunders, B. R.; Laajam, N.; Daly, E.; Teow, S.; Hu, X. H.; Stepto, R. *Adv. Colloid Interface Sci.* **2009**, *147−148*, 251−262.
(44) Ono, Y.; Shikata, T. *J. Am. Chem. Soc.* **2006**, *128*, 10030−10031.
(45) Shibayama, M.; Ikkai, F.; Inamoto, S.; Nomura, S.; Han, C. C. *J. Chem. Phys.* **1996**, *105*, 4358−4366.
(46) Jones, C. D.; Lyon, L. A. *Macromolecules* **2000**, *33*, 8301−8306.
(47) Zhou, S. Q.; Chu, B. *J. Phys. Chem. B* **1998**, *102*, 1364−1371.
(48) Imaz, A.; Forcada, J. *Eur. Polym. J.* **2009**, *45*, 3164−3175.
(49) Kerker, M. In *The scattering of light and other electromagnetic radiation*; Academic Press: New York, 1969.
(50) Duracher, D.; Elaissari, A.; Pichot, C. *J. Polym. Sci., Part A: Polym. Chem.* **1999**, *37*, 1823−1837.
(51) Vivero-Escoto, J. L.; Slowing, I. I.; Trewyn, B. G.; Lin, V. S. Y. *Small* **2010**, *6*, 1952−1967.
(52) Xu, H. F.; Meng, F. H.; Zhong, Z. Y. *J. Mater. Chem.* **2009**, *19*, 4183−4190.
(53) Shimoni, O.; Postma, A.; Yan, Y.; Scott, A. M.; Heath, J. K.; Nice, E. C.; Zelikin, A. N.; Caruso, F. *ACS Nano* **2012**, *6*, 1463−1472.
(54) Duncan, R. *Nat. Rev. Drug Discovery* **2003**, *2*, 347−360.
(55) Barenholz, Y.; Amselem, S.; Goren, D.; Cohen, R.; Gelvan, D.; Samuni, A.; Golden, E. B.; Ga-bizon, A. *Med. Res. Rev.* **1993**, *13*, 449−491.
(56) Choucair, A.; Soo, P. L.; Eisenberg, A. *Langmuir* **2005**, *21*, 9308−9313.
(57) Hoare, T.; Pelton, R. *Langmuir* **2008**, *24*, 1005−1012.
(58) Karg, M.; Hellweg, T. *J. Mater. Chem.* **2009**, *19*, 8714−8727.
(59) Yan, E. Y.; Ding, Y.; Chen, C. J.; Li, R. T.; Hu, Y.; Jiang, X. Q. *Chem. Commun.* **2009**, *45*, 2718−2720.
(60) Zhang, Q.; Liu, F.; Nguyen, K. T.; Ma, X.; Wang, X. J.; Xing, B. G.; Zhao, Y. L. *Adv. Funct. Mater.* **2012**, *22*, 5144−5156.
(61) Gaulding, J. C.; Smith, M. H.; Hyatt, J. S.; Fernandez-Nieves, A.; Lyon, L. A. *Macromolecules* **2012**, *45*, 39−45.
(62) Li, Y. L.; Zhu, L.; Liu, Z. Z.; Cheng, R.; Meng, F. H.; Cui, J. H.; Ji, S. J.; Zhong, Z. Y. *Angew. Chem., Int. Ed.* **2009**, *48*, 9914−9918.
(63) Cui, J. W.; Yan, Y.; Wang, Y. J.; Caruso, F. *Adv. Funct. Mater.* **2012**, *22*, 4718−4723.